

## EXPERIMENTAL INVESTIGATION OF MICROSTRUCTURAL AND MECHANICAL PROPERTIES OF STAINLESS STEEL 202 JOINT USING TIG WELDING

Mahavir Rathore<sup>1</sup> Shailesh Dewangan<sup>1\*</sup> Joji Thomas<sup>1</sup> and Nitin Nayak<sup>1</sup>

<sup>1</sup>Department of Mechanical Engineering Chouksey Engineering College Bilaspur Chhattisgarh

\*Email id- [shaileshd@cecbilaspur.ac.in](mailto:shaileshd@cecbilaspur.ac.in)

\*Corresponding author: Shailesh Dewangan

\*Email id- [shaileshd@cecbilaspur.ac.in](mailto:shaileshd@cecbilaspur.ac.in)

### Abstract

Stainless Steel 202 is a popular material in various industrial applications due to its excellent corrosion resistance, high strength, and cost-effectiveness compared to other stainless-steel grades like 304 or 316. So, the current experimental study is to investigate the Gas Tungsten Arc Welding (GTAW;) process for welding stainless steel 202 (SS202) using an SS310 filler rod, with the goal of achieving the best mechanical properties and minimal heat-affected zone (HAZ). The welding parameters considered are the main current, start current, end current, and pulse (Hz), and the Taguchi orthogonal array L<sub>9</sub> was employed to systematically investigate their impact on weld quality. The analysis of mechanical properties and microstructure provides a clear understanding of the relationship between the chosen welding parameters and the weld performance. The final result should yield a combination of settings that offers the best compromise between weld strength, minimized HAZ, and improved overall weld quality.

**Keywords:** Mechanical Properties; SS202; Taguchi Design; TIG Welding; Elongation

### 1. Introduction:

Welding technology has seen significant advancements over the years, largely driven by its widespread applications across various industries. Among the many welding processes developed, Tungsten Inert Gas welding has garnered considerable interest due to its versatility and effectiveness[1], [2]. Stainless Steel 202 is widely utilized in various industrial applications because of its exceptional corrosion resistance, high strength, and cost-effectiveness compared to other stainless-steel grades, such as 304 or 316. This combination of properties makes it an attractive choice for applications where durability and affordability are essential[3].

The Microstructural observation reveals the formation of martensite in the interface region of the weldment [4], [5]. A tensile test, conducted using a Universal Testing Machine, indicates that the weldment with ER316L filler exhibits a higher tensile strength compared to the other filler materials [6]. Wang et. al [7] suggested the heat-affected zone (HAZ) expands, and the grains become coarser. After TIG remelting, the TIG-remelted joints exhibited a 4.5% increase in tensile strength and a 20.0% increase in elongation in TIG welding. In TIG welding, the high temperatures involved often lead to significant distortion and residual stress in the welded joint [8]. The TIG weldments of Inconel 718 and SS316L displayed exceptional mechanical and metallurgical qualities when exposed to high temperatures [9]. To address these challenges and develop a high-quality weld with controlled residual stress and deformation, we employ Welding Simulation using Finite Element Methodology (FEM)[10]. Simulation of the Impact of Welding Parameters on Weld Pool Behaviour in a TIG-MIG Hybrid Welding Process[11].

Due to its limited penetration depth, this process has a narrow range of industrial applications and is mainly used for working with sheet metal[12]. The examination of welds involved radiographic analysis and a detailed assessment of mechanical properties. The mechanical properties of the welded joints were characterized through tensile tests, which provided data on yield stress, tensile strength, and strain at maximum stress[13]. examines the impact of friction stir processing on TIG welding with fillers for dissimilar aluminium alloys. It investigates the mechanical characterization, finite element modelling, and mathematical equations governing heat transfer in TIG + FSP welded joints[14].

The objective of this work is to maximize welding strength and tensile load while minimizing elongation by optimizing various welding parameters using the  $L_9$  orthogonal array based on Taguchi's design of experiments. Additionally, it aims to identify the optimal combination of parameters, such as main current, end current, start current, and pulse, to achieve minimal cracks and surface defects in the microstructure.

## 2. Materials and Methods:

### 2.1: Selection of base metal and filler rod:

In this work, the material selected for the experimental process is stainless steel 202 (SS202) with dimensions  $700 \times 120 \times 3$  mm which is shown in Fig 1. SS202 is known for its balance of strength and corrosion resistance, which is attributed to its chromium concentration. This type of stainless steel is frequently chosen for applications that require both durability and dependability in challenging environments. For welding purposes, the filler rod selected is SS310, which has superior heat resistance properties compared to SS202. The use of SS310 as the filler material could enhance the performance of the welded joint, especially in high-temperature conditions.

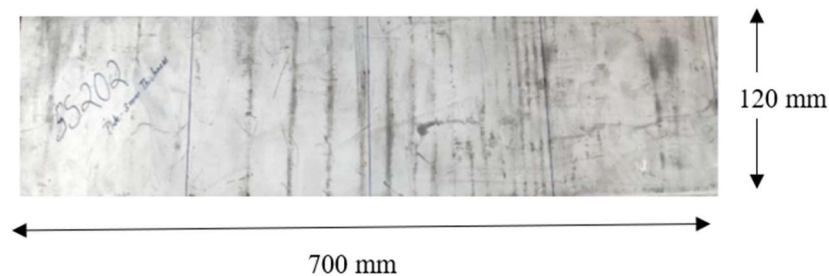


Fig. 1 Materials SS202

The emphasis on higher chromium concentration increasing corrosion resistance is key to understanding why SS202 remains a reliable choice for industries requiring resilient and strong materials. The experimental process involving SS202 and SS310 aims to investigate the welding characteristics and the mechanical integrity of the joint formed between these two materials.

### 2.2: Sample preparation

The sample preparation process described is crucial for ensuring the accuracy and reliability of the experimental outcomes. Beginning with the use of a hand grinder with a cutter blade, followed by surface polishing, ensures that the workpiece (SS202) is shaped with precision and has a smooth surface for optimal welding. Surface quality is essential for maintaining consistency in the welding process and in minimizing any potential defects that could arise from irregularities. The choice of a Fronius TIG

welding machine highlights the commitment to precision, as TIG (Tungsten Inert Gas) welding is known for producing high-quality welds with excellent control over the heat input, making it ideal for stainless steel. This machine's application ensures that the integrity of the welded joint is preserved, which is vital for the accurate evaluation of the material's performance, especially under conditions where strength and corrosion resistance are tested.

By adhering to such a detailed and systematic approach in both sample preparation and welding, the study ensures that subsequent assessments of the material's mechanical properties, microstructure, and corrosion resistance will be based on a well-prepared and reliably welded sample. This method ensures that the material's true characteristics can be evaluated with minimal external interference from imperfections or inconsistencies during sample preparation or welding.

The chemical composition of both the base metal (BM) and filler materials plays a critical role in determining the mechanical properties, corrosion resistance, and overall performance of the welded joint. Table 1 is showing the chemical compositions (in weight percentages) for stainless steel 202 (SS202) as the base metal and stainless steel 310 (SS310) as the filler material, which are often used in such experimental setups.

**Table 1 Chemical Composition of Base Metal and filler material**

Element	Composition (wt.%)	
	Base Metal	Filler Material
Chromium (Cr)	17.0–19.0	24.0–26.0
Nickel (Ni)	4.0–6.0	19.0–22.0
Manganese (Mn)	7.5–10.0	≤ 2.0
Carbon (C)	≤ 0.15	≤ 0.25
Silicon (Si)	≤ 1.0	≤ 1.5
Phosphorus (P)	≤ 0.06	≤ 0.045
Sulfur (S)	≤ 0.03	≤ 0.03
Iron (Fe)	Balance	Balance

### 2.3: Experimentation

The use of Taguchi's orthogonal array theory for the experimental observations and analysis ensures a robust and efficient design of experiments (DOE), reducing the number of experiments while capturing essential information about process parameters. In this case, the L<sub>9</sub> orthogonal array was employed, meaning that 9 experimental runs were conducted, with each run representing a unique combination of control factors or parameters. The machining parameters and their levels are presented in Table 2.

**Table 2 Machining Parameters and their levels**

Control Parameters	Unit	Levels		
		Low	Medium	High
Main Current	A	75	90	105
Start Current	%	90	110	130
End Current	%	50	60	70
Pulse	Hz	0	25	50

### 2.4 Microstructural properties

After the welding process, the specimens were sectioned to dimensions of 10 × 10 × 3 mm for microstructure analysis. The weld samples were polished using silicon carbide paper in successive grit

sizes of 200, 400, 800, 1200, 1500, 2000, and 2500. This was followed by velvet cloth polishing with a  $0.75\ \mu\text{m}$  alumina slurry. The polished samples were then subjected to ultrasonic cleaning. Various regions of the weld were analysed, and a metallographic examination was performed using an optical microscope.

### 2.5 Mechanical properties

The tensile properties of the joints, including yield strength, ultimate tensile strength, and percentage elongation, were evaluated using a universal testing machine (UTM) under typical environmental conditions. For the square butt joint, torque was calculated. The test specimen measured  $80 \times 25 \times 3$  mm. sample size of specimen is shown in Fig. 2.

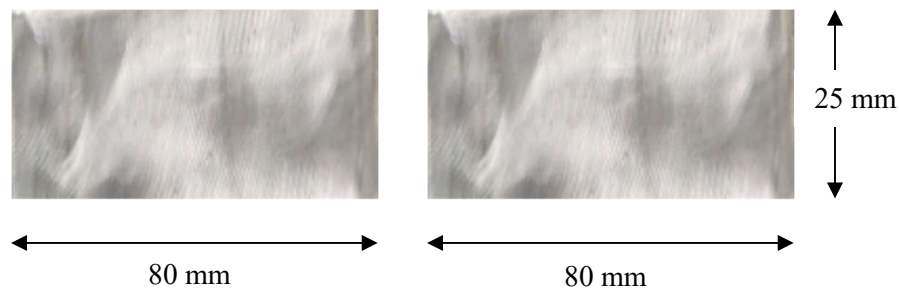


Fig. 1 Workpiece for square butt joint

## 3. Results and discussion

### 3.1 Microstructural examination

SEM analysis was conducted to detect any internal defects in the specimen. In this study, the specimen that produced the best results was analysed, revealing no internal cracks. The Fig. 3 below shows images of the weld region of the polished SS202 steel samples from various angles. Microscopic examination confirmed the absence of internal cracks or microstructural defects in the welded zone, demonstrating a high level of structural integrity and weld quality. This suggests effective fusion and minimal stress concentrations within the welded region. The lack of internal cracks indicates the weld's resilience to potential failure mechanisms, thereby enhancing the overall durability and performance of the welded component. These findings highlight the significance of precise welding procedures and rigorous quality control measures to ensure the integrity and reliability of welded structures under operational conditions.

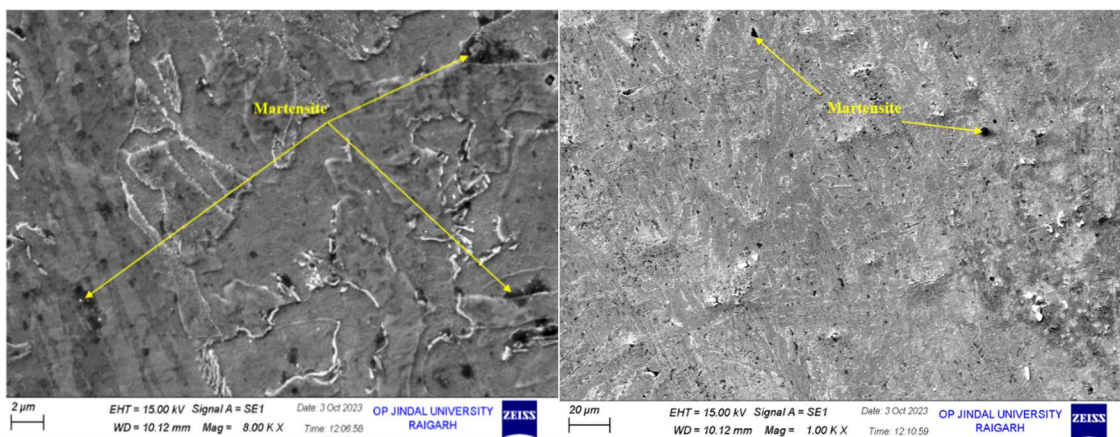


Fig. 2 SEM image of base metal

### 3.2 Tensile test & torque calculation

As shown in Fig. 4, the experimental setup for the tensile test was performed using a Universal Testing Machine (UTM). A total of nine experiments were conducted using an L<sub>9</sub> orthogonal array (OA) based on the Taguchi design of experiments. For these experiments, nine samples were prepared with lap joints to measure the tensile test and calculate the elongation. Additionally, nine samples were prepared with square butt joints for torque calculation. The experimental observations and results are summarized in Table 3.

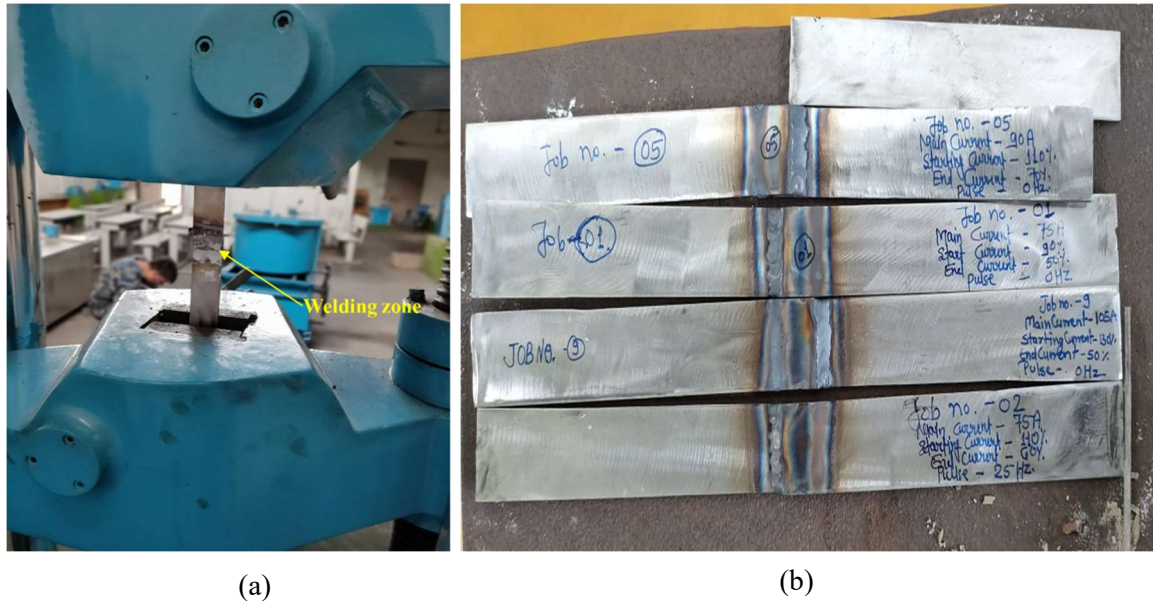


Fig. 3 (a) Tensile test experimental setup, (b) welded base metal

In Table 3, the experimental observations and analysis are based on Taguchi's orthogonal array theory, utilizing an L<sub>9</sub> orthogonal array for the entire SS202 steel welding experimentation. This array involved nine experimental runs, with the corresponding outputs evaluated using Taguchi optimization techniques. The load on the welding joint and the tensile load were measured using the specified instruments, with these measurements serving as input parameters for the Taguchi optimization method. As a result, nine experiments were conducted according to this orthogonal array, and the corresponding output data were recorded sequentially. The tensile strength of the workpieces was measured, and the mean values of these measurements were calculated.

Table 3 Experimental observed value

Sr. No.	Main Current (A)	Start Current (%)	End Current (%)	Pulse (Hz)	Tensile Load (KN)	Elongation (mm)	Torque (Nm)
1	75	90	50	0	92.8	28	16.2
2	75	110	60	25	105	30	16.8
3	75	130	70	50	108	48	21.6
4	90	90	60	50	101	40	15.7
5	90	110	70	0	88	22	13.4
6	90	130	50	25	106.5	48	18.2
7	105	90	70	25	107.3	51	19.9
8	105	110	50	50	96	24	17.3

9	105	130	60	0	99.4	35	19.2
---	-----	-----	----	---	------	----	------

### 3.3 Influence of welding parameter on tensile test and elongation

The primary objective of this analysis was to maximize welding strength and tensile load while minimizing elongation, utilizing the "larger-the-better" optimization criterion. According to the main effect plot for tensile strength (Fig. 5), it was observed that as the main current increased up to 90 A, the tensile strength initially decreased, but with further increases in current, the tensile strength began to rise. A similar pattern was noted for the start current. In contrast, the end current and pulse exhibited a different behaviour, where tensile strength first increased and then decreased with higher values.

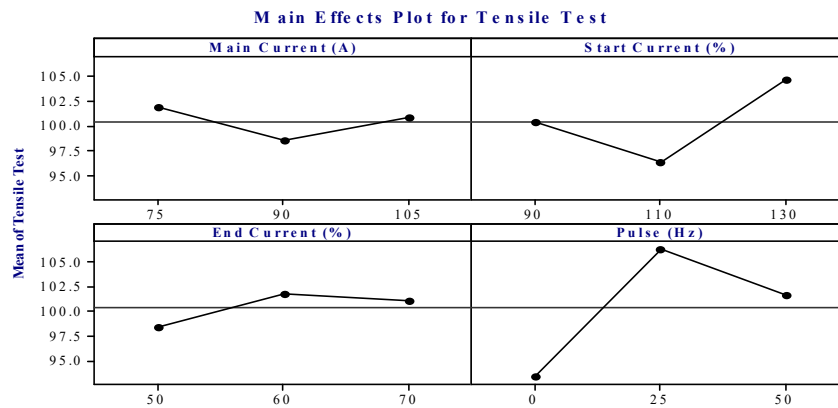


Fig. 4 Main effects plot for Tensile Test

The analysis of variance for tensile strength, presented in Table 4, revealed that the main current and end current contributed minimally to the response variations. However, the pulse was found to have a significant impact on the tensile strength, indicating its critical role in optimizing welding performance.

Table 4 Analysis of Variance for Tensile Test

Source	DF	Seq SS	Adj MS	F	P	% Contribution
Main Current (A)	2	18.62	9.308	0.18	0.847	4.70
End Current (%)	2	18.94	9.468	0.18	0.845	4.78
Pulse (Hz)	2	255.05	127.524	2.47	0.288	64.41
Residual Error	2	103.36	51.681			26.10
Total	8	395.96				
S = 7.189 R-Sq = 73.9% R-Sq(adj) = 0.0%						

The analysis of the elongation from Fig. 6 and Table 5 suggests that the main current and end current have minimal effects on elongation, with contributions of 0.30% and 8.27%, respectively. This implies that changes in these parameters do not significantly influence elongation. The pulse, however, shows a significant effect. It appears that elongation increases with an increase in pulse frequency up to 25 Hz, showing a direct proportionality. Beyond 25 Hz, however, elongation decreases as the pulse frequency increases, indicating an inverse relationship between elongation and pulse in the 25-50 Hz range.

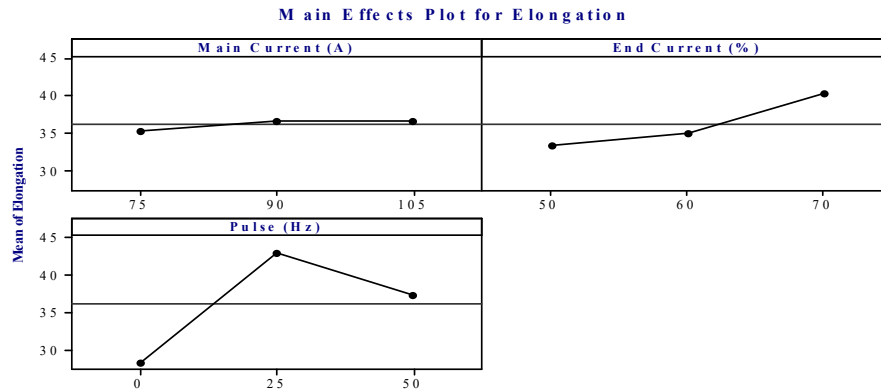


Fig. 5 Main Effect Plot for Elongation

This behaviour could be due to various factors, such as material behaviour under different frequencies, heat generation, or the dynamics of the process being studied. The results highlight the critical role of pulse frequency in determining elongation and suggest that there might be an optimal pulse frequency around 25 Hz for maximizing elongation.

Table 5 Analysis of Variance for Elongation

Source	DF	Seq SS	Adj MS	F	P	% Contribution
Main Current (A)	2	3.556	1.778	0.01	0.994	0.30
End Current (%)	2	80.222	40.111	0.14	0.874	8.27
Pulse (Hz)	2	328.222	164.111	0.59	0.629	33.85
Residual Error	2	557.556	278.778			57.51
Total	8	969.556				
S = 16.70 R-Sq = 42.5% R-Sq(adj) = 0.0%						

#### 4. Conclusions

In this study, we aimed to optimize the welding process to achieve maximum welding strength and tensile load while minimizing elongation. Our analysis revealed that pulse parameters play a significant role in influencing tensile load, elongation, and torque, whereas other machining parameters such as main current, start current, and end current do not have a substantial impact. Furthermore, microstructural analysis confirmed the absence of internal cracks or defects within the welded zone, indicating a high level of structural integrity and weld quality. SEM imaging also supported these findings, showing different phases without any internal cracks. This research underscores the critical influence of pulse in welding processes and confirms the superior quality of the welds produced under the optimized conditions.

#### References

- [1] S. C. Juang and Y. S. Tarng, "Process parameter selection for optimizing the weld pool geometry in the tungsten inert gas welding of stainless steel," *J. Mater. Process. Technol.*, vol. 122, no. 1, pp. 33–37, 2002, doi: 10.1016/S0924-0136(02)00021-3.
- [2] O. S. Ogbonna, S. A. Akinlabi, N. Madushele, O. S. Fatoba, and E. T. Akinlabi, "Grey-based taguchi method for multi-weld quality optimization of gas metal arc dissimilar joining of mild steel and 316 stainless steel," *Results Eng.*, vol. 17, no. February, p. 100963, 2023, doi: 10.1016/j.rineng.2023.100963.

- [3] S. Tiwari and S. Shukla, "Optimizing GTAW Process Parameters for SS202 Welding using the Taguchi Method," *J. Propuls. Technol.*, vol. 45, no. 2, pp. 2851–2863, 2024.
- [4] H. Cai, L. Xu, L. Zhao, Y. Han, and X. Guo, "Microstructure and mechanical properties of 9Cr-3Co-2.9 W-CuNbV steel welded joints processed by different tungsten inert gas (TIG) welding," *Mater. Charact.*, vol. 199, no. February, 2023, doi: 10.1016/j.matchar.2023.112840.
- [5] H. Wang, S. Chang, Z. Zhou, and W. Wang, "Effect of TIG remelting on the microstructure, mechanical properties, and corrosion behavior of 5052 aluminum alloy joints in MIG welding," *J. Mater. Res. Technol.*, vol. 32, no. July, pp. 2255–2267, 2024, doi: 10.1016/j.jmrt.2024.08.087.
- [6] S. Ambade *et al.*, "Experimental investigation of microstructural, mechanical and corrosion properties of 316L and 202 austenitic stainless steel joints using cold metal transfer welding," *J. Mater. Res. Technol.*, vol. 27, no. November, pp. 5881–5888, 2023, doi: 10.1016/j.jmrt.2023.11.091.
- [7] Z. Zhang, Z. J. Tan, Y. F. Wang, D. X. Ren, and J. Y. Li, "The relationship between microstructures and mechanical properties in friction stir lap welding of titanium alloy," *Mater. Chem. Phys.*, vol. 296, p. 127251, 2023, doi: <https://doi.org/10.1016/j.matchemphys.2022.127251>.
- [8] K. R. Kavitha, G. Kumar, G. Lakshmi Srinivas, J. Lilly Mercy, P. Sivashankari, and N. Joy, "Evaluation study of mechanical properties of dissimilar materials through TIG welding process," *Mater. Today Proc.*, vol. 44, pp. 3894–3897, 2021, doi: 10.1016/j.matpr.2020.12.1107.
- [9] B. Yelamasetti *et al.*, "Mechanical Characterization and Microstructural Evolution of Inconel 718 and SS316L TIG Weldments at High Temperatures," *J. Mater. Res. Technol.*, vol. 32, no. July, pp. 196–207, 2024, doi: 10.1016/j.jmrt.2024.07.157.
- [10] H. Arora, K. M. Basha, D. N. Abhishek, and B. Devesh, "Welding simulation of circumferential weld joint using TIG welding process," *Mater. Today Proc.*, vol. 50, pp. 923–929, 2021, doi: 10.1016/j.matpr.2021.06.315.
- [11] X. Wu, X. Zhao, J. Chen, Z. Zhang, and C. Wu, "Simulation of the influence of welding parameters on weld pool behavior during a TIG-MIG hybrid welding process," *J. Manuf. Process.*, vol. 79, no. December 2021, pp. 460–475, 2022, doi: 10.1016/j.jmapro.2022.05.007.
- [12] G. Sharma, R. Tyagi, Priyanshu, and P. Sharma, "Variants of TIG welding process for improvement of weld penetration depth - A review," *Mater. Today Proc.*, vol. 64, pp. 1362–1366, 2022, doi: 10.1016/j.matpr.2022.04.266.
- [13] R. Casanueva, C. Brañas, F. J. Diaz, F. J. Azcondo, D. Ferreño, and J. Setien, "Characterization of an energy efficient pulsed current TIG welding process on AISI 316 and 304 stainless steels," *Heliyon*, vol. 9, no. 9, pp. 1–13, 2023, doi: 10.1016/j.heliyon.2023.e19819.
- [14] H. Mehdi and R. S. Mishra, "Effect of friction stir processing on mechanical properties and heat transfer of TIG welded joint of AA6061 and AA7075," *Def. Technol.*, vol. 17, no. 3, pp. 715–727, 2021, doi: 10.1016/j.dt.2020.04.014.